Simulated Moving-Bed Reactor: Reactive–Separation Regions

Mirjana Minceva and Alirio E. Rodrigues
Laboratory of Separation and Reaction Engineering (LSRE), Dept. of Chemical Engineering, Faculty of Engineering, University of Porto, 4200-465 Porto, Portugal

DOI 10.1002/aic.10532
Published online July 19, 2005 in Wiley InterScience (www.interscience.wiley.com).

This work focuses on the design of a simulated moving-bed rector (SMBR) where reaction $A \rightarrow B + C$ takes place. The reactive–separation regions were determined for two reactive systems: (1) inversion of sucrose, with enzyme introduced in the unit through the eluent stream and Michaelis–Menten reaction kinetics, and (2) $A \rightarrow B + C$ reaction, with immobilized enzyme and linear reaction kinetic law. In both systems the reaction species exhibit linear adsorption isotherms. The steady-state equivalent true moving-bed reactor (TMBR) analogy was applied in the algorithm used for determination of the reactive–separation regions. The influence of the mass-transfer limitation, reaction rate, product purities, reactant Henry constant, and SMBR configuration on the shape and position of reactive–separation regions was analyzed. It was shown that in certain conditions the reactive–separation regions extended out of the separation regions obtained for nonreactive SMB for product (B and C) separation. © 2005 American Institute of Chemical Engineers *AIChE J,* 51: 2737–2751, 2005

Keywords: simulated moving-bed reactor, reactive–separation region, irreversible reaction, sucrose inversion, Michaelis–Menten

Introduction

Reactive separations combine the generally separated and sequential unit operations of reaction and separation into a simultaneous single operation.[1] The main advantages of the reactive–separation processes are reduction of the operating and capital cost, as well as improvement of the reaction and separation efficiency. The simulated moving-bed reactor (SMBR) technology is a combination of the chemical or biochemical reaction with a simulated moving bed (SMB) chromatographic separator. The SMBR is a continuous countercurrent process that brings advantages in view of the separation/reaction, as increased conversion and/or product purity, increased driving force by countercurrent operation, and overcomes the difficulties connected to the solid abrasion and handling by simulation of the countercurrent flow. The potential applications of this technology are in (1) equilibrium-limited reversible reaction where the removal of products as they are formed allows achieving conversions well beyond equilibrium values; (2) reactions in series or in parallel, where the desired intermediate species could be separated selectively; and (3) reactions with inhibiting or poisoning product, where its removal from the reaction medium could promote yield improvement.

The first application of reactive SMB in a zeolite-catalyzed alkylation reaction dates back to the 1970s.[2] In the last decade the SMBR has been the subject of considerable attention mainly because of the increased interest in the area of process intensification and successful entrance of the SMB technology in the pharmaceutical industry.

The laboratory-scale SMBR has been used effectively to carry equilibrium-limited reversible reaction in the liquid phase, such as esterifications,[3-7] etherifications,[8] alkylations,[9] and acetalization[10]; as well as gas-phase reactions: hydrogenations,[11,12] partial oxidation of methane,[13] and oxidative coupling of methane.[11,14,15] The biochemical reactions involving

Correspondence concerning this article should be addressed to A. E. Rodrigues at arodrig@fe.up.pt.

sugars have been also investigated extensively, as glucose isomerization,[16-19] inversion of sucrose by enzyme invertase,[20-22] production of high molecular weight dextran,[21] enzymatic conversion of glucose to glucose-6-phosphate,[23] hydrolysis of lactose and maltose,[24,25] and the production of lactosucrose.[26]

Even though a reasonable amount of experimental and numerical studies on SMBR have been published, there is still no reported application of SMBR in the chemical process industry. The determination of SMBR optimal design parameters and operating conditions is decisive in the study of the process viability at the industrial level.

Few studies have been reported on the design and optimization of SMBR, based on either simulation[22,27] or single[22,28] or multiobjective optimization.[18,29-31]

Dünnebier et al.[28] presented a novel optimization and design strategy for an SMBR based on a rigorous process model and a detailed cost function. Azevedo and Rodrigues[22] adopted the algorithm proposed by Biressi et al.[32] to design both the operating and the geometric parameters of a reactive SMB for sucrose inversion in the presence of mass-transfer resistance.

Design criteria for both irreversible ($A \rightarrow B + C$) and reversible reaction ($A \leftrightarrow B + C$), where the reactant adsorption affinity is between those of the products, based on the TMBR equivalence and the equilibrium theory have been developed.[33,34] A novel analytical solution of equivalent TMBR, for the reaction of type $A \rightarrow B + C$, in the presence of intraparticle mass-transfer resistance described by linear driving force (LDF) model has been recently applied in the design of the SMBR reactive–separation regions.[35]

The design of an SMBR system is associated with several important objectives [productivity, eluent (desorbent) consumption, adsorbent/catalyst inventory] that require optimization, along with the constraints (product purity, conversion, recovery) that must be satisfied at the same time. It has been shown that genetic algorithms can be useful in the optimization of these complex units.[18,29-31] In multiobjective optimization there is an entire set of equally good optimal solutions (Pareto optimal solutions). Often, it remains difficult to draw general conclusions about the optimal design of the SMBR units because the choice of one solution over the other requires additional knowledge of the problem.

In this work the design of SMBR where the reaction $A \rightarrow B + C$ takes place was studied. The steady-state equivalent true moving-bed reactor (TMBR) analogy was implemented in the algorithm used for determination of the reactive–separation regions. Two reactive systems were considered: (1) inversion of sucrose, with enzyme introduced in the unit through the eluent stream and Michaelis–Menten reaction kinetics, and (2) $A \rightarrow B + C$ reaction, with immobilized enzyme and linear reaction kinetic law. In both systems the reaction species exhibit linear adsorption isotherms.

The design of the SMBR for sucrose inversion is presented in the first part of this paper. The bilinear driving force (bi-LDF) equivalent TMBR model is used to study the influence of mass-transfer resistance, product purities, SMBR configuration, and enzyme concentration on the reactive–separation regions of SMBR for sucrose inversion. The effect of the enzyme concentration and reactant Henry constant on the reactive–separation regions was also studied in the absence of the mass-transfer resistance.

In the second part, the design of SMBR for a general type of irreversible reaction $A \rightarrow B + C$, in the absence of mass transfer, is discussed. Special attention is given to the influence of the reactant (A) adsorption affinity on the reactive–separation regions.

SMBR for Sucrose Inversion

The SMBR for the enzymatic inversion of sucrose and separation of fructose from glucose was considered. The inversion of sucrose by enzyme invertase is an irreversible reaction:

$$\text{Sucrose} \xrightarrow{\textit{invertase}} \text{Fructose} + \text{Glucose}$$

The reaction rate is not influenced by product accumulation. Meurer et al.[36] showed that the SMBR, when applied even for irreversible reactions, provides better conversion and product purities than the conventional processes. Also, the simultaneous inversion and product separation overcomes the problems associated with substrate inhibition.[21]

The SMBR, presented in Figure 1a, consists of a set of columns packed with cation-exchange resin (DOWEX Monosphere 99/Ca, by Sigma) and arranged in a closed circuit, with two inlet streams (feed and eluent) and two outlet streams (extract and raffinate). Sucrose (A) solution in water is used as feed and water is used as eluent. The enzyme is introduced in the system diluted in the eluent (buffer solution). The fructose (B) is collected in the extract as a more strongly adsorbed component and glucose (C) is collected in the raffinate as less strongly adsorbed component. At regular time intervals, the introduction and withdrawal points are advanced one bed ahead in the direction of fluid flow; the countercurrent motion of the solid adsorbent is simulated and the solid velocity is equal to the length of a column divided by the switching time. When the number of switches is equal to the number of columns one cycle is completed.

The SMBR principle of operation may be more clearly understood by considering the equivalent representation of a true moving-bed reactor (TMBR). In the TMBR (Figure 1b) the inlet and outlet points are kept unchanged and the solid phase (adsorbent) really moves in the direction opposite to that of the fluid phase. The TMBR representation also provides a simpler model for the purposes of process prediction and design.

Mathematical model

The bi-LDF steady-state equivalent TMBR model has been used to describe the SMBR unit behavior. The model assumes axially dispersed flow for the fluid phase and plug flow for the solid phase, diffusion through the external film, and intraparticle mass transfer represented by means of a bilinear driving force.[22] The reaction of sucrose inversion is described by the Michaelis–Menten equation. Sucrose is assumed to react in the interparticle fluid phase and at the surface of the resin as a result of the immobilized enzyme adsorbed at its exterior surface. The reaction products, glucose and fructose, have linear adsorption isotherms. Sucrose adsorption into the adsor-

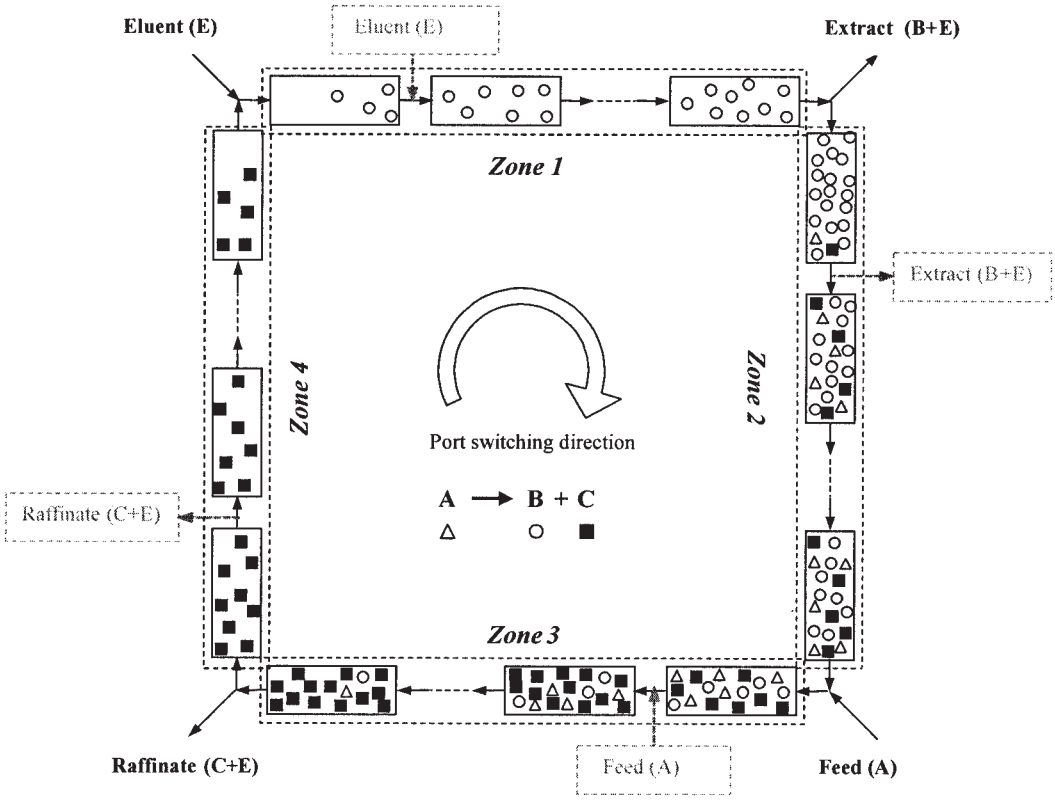

a)

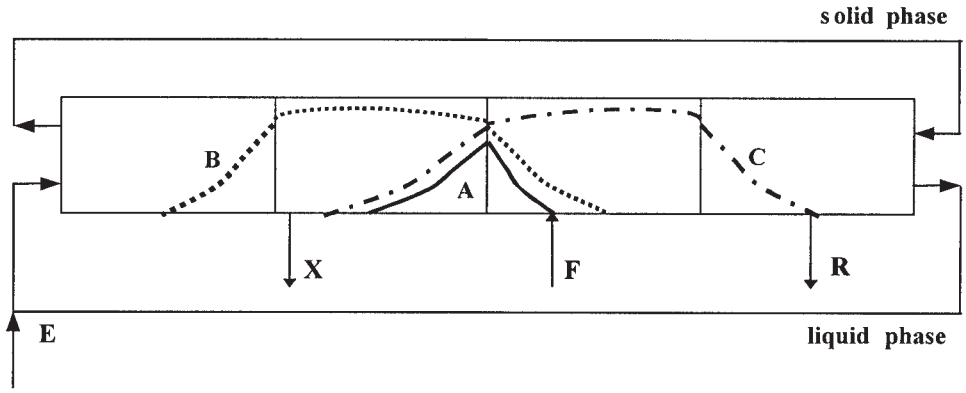

b)

Figure 1. (a) SMBR schematic diagram and (b) TMBR schematic diagram.

bent particles was not considered in the model because it has been observed experimentally that the adsorption constant of sucrose is nearly equal to the particle porosity.[37]

The model equations are summarized in Table 1. All mass-balance equations are written in terms of mass rather than moles. Model equations were numerically solved by gPROMS.[38] The system of ordinary differential and algebraic equations (DAE) was solved by DASOLV solver incorporated in gPROMS. The axial domain is discretized using a third-order orthogonal collocation method in finite elements (OCFEM). In the case of significant mass-transfer limitation 20 finite elements per column were used; otherwise, 200 elements per column were considered. For a typical simulation, CPU times of about 0.5 s in the case of mass-transfer limitation and 20 s in an absence of mass-transfer limitations were required on Pentium IV 2300 MHz processor with 2 GB RAM memory.

Reactive–separation region in the presence of mass-transfer limitation

The reactive–separation regions of the SMBR for sucrose inversion were determined with the bi-LDF steady-state equivalent TMBR model. The influence of the (1) product purities

Table 1. Bi-LDF Steady-State Equivalent TMBR Model Equations

Mass balance in the interparticle liquid phase in zone j

$$\frac{\gamma_j}{\mathrm{Pe}_j}\frac{d^2C_{i,j}}{dx^2} - \gamma_j\frac{dC_{i,j}}{dx} - \nu\frac{\mathrm{Bi}_{m_j}}{\mathrm{Bi}_{m_j}+5}\alpha_{p_{i,j}}(C_{i,j} - \langle C_p\rangle_{i,j}) + \alpha_{r_j}(1 + \nu K_{Enz})\left(\frac{\sigma_i R_j}{k_r}\right) = 0 \qquad (i = A, B, C)$$

$$\frac{1}{\mathrm{Pe}_j}\frac{d^2C_{i,j}}{dx^2} - \frac{dC_{i,j}}{dx} = 0 \qquad (i = Enz)$$

where

$$R_j = k_r\frac{C_{s,j}\times C_{e,j}}{K_{mm}+C_{s,j}} \qquad \sigma_i = \begin{cases} -1 & \text{if } i \text{ is } A \\ +0.526 & \text{if } i \text{ is } B \text{ or } C \end{cases}$$

Mass balance in the liquid phase within particle pores in zone j

$$\frac{\partial\langle C_p\rangle_{i,j}}{\partial x} + \frac{\mathrm{Bi}_{mj}}{5+\mathrm{Bi}_{mj}}\frac{\alpha_{pi,j}}{\varepsilon_p}(C_{i,j} - \langle C_p\rangle_{i,j}) - \frac{\alpha_{\mu i,j}}{\varepsilon_p}[K_i\langle C_p\rangle_{i,j} - \langle\langle q\rangle\rangle_{i,j}] = 0 \qquad (i = A, B, C)$$

Mass balance in the solid phase within the adsorbent particles in zone j

$$\frac{\partial\langle\langle q\rangle\rangle_{i,j}}{\partial x} + \alpha_{\mu_{i,j}}[K_i\langle C_p\rangle_{i,j} - \langle\langle q\rangle\rangle_{i,j}] = 0 \qquad (i = A, B, C)$$

Boundary conditions for a given zone j are

$$C^{in}_{i,j} = C_{i,j}(0) - \frac{1}{\mathrm{Pe}_j}\frac{\partial C_{i,j}}{\partial x} \qquad \frac{\partial C_{i,j}}{\partial x}(1) = 0 \qquad (i = A, B, C, Enz)$$

$$\langle C_p\rangle_{i,j}(1) = \langle C_p\rangle_{i,j+1}(0) \qquad \langle\langle q\rangle\rangle_{i,j}(1) = \langle\langle q\rangle\rangle_{i,j+1}(0) \qquad (i = A, B)$$

Dimensionless groups

$$\gamma_j = \frac{U'_{F_j}}{U_S} \qquad \mathrm{Pe}_j = \frac{U'_{F_j}L_j}{D_{ax_j}} \qquad \nu = \frac{(1-\varepsilon)}{\varepsilon} \qquad \sigma_i = \frac{\text{Mol. weight of } B \text{ (or } C)}{\text{Mol. weight of } A}$$

$$\alpha_{pi,j} = \frac{k_{pi}L_j}{U_S} \qquad \alpha_{rj} = \frac{k_rL_j}{U_S} \qquad \alpha_{\mu i,j} = \frac{k_{\mu i}L_j}{U_S} \qquad \mathrm{Bi}_{mj} = \frac{k_{fj}R_p}{D_{pe}}$$

Node mass balances

Eluent node
$$C^{in}_{i,l} = \frac{Q'_4}{Q'_1}C_{i,4}(1) + \frac{Q_E}{Q'_1}C_{i,E}$$

Feed node
$$C^{in}_{i,3} = \frac{Q'_2}{Q'_3}C_{i,2}(1) + \frac{Q_F}{Q'_3}C_{i,F}$$

Extract node
$$C^{in}_{i,2} = C_{i,1}(1)$$

Raffinate node
$$C^{in}_{i,4} = C_{i,3}(1)$$

and (2) enzyme concentration in the eluent, on the reactive–separation region size and position was studied. In both cases the required conversion was set at the minimum of 99%. The expressions used to calculate the product purities and reactant conversion are given in Table 2.

Adsorption equilibrium data, mass transfer, and reaction parameters for sucrose inversion and glucose-fructose adsorptive separation, provided by Azevedo and Rodrigues,[22] are presented in Table 3.

The values of the γ_1 and γ_4 were calculated according to the equilibrium theory for linear equilibrium nonreactive systems[39]:

$$\gamma_1 > \nu(K_B + \varepsilon_p) = 0.795$$

Table 2. Expressions Used for SMBR Performance

Performance	Expression
Extract purity (%)	$PUX = 100 \times \dfrac{C_{B,E}}{C_{A,E}+C_{B,E}+C_{C,E}}$
Raffinate purity (%)	$PUR = 100 \times \dfrac{C_{C,R}}{C_{A,R}+C_{B,R}+C_{C,R}}$
Conversion (%)	$X = 100 \times \dfrac{C_{A,F}Q_F - (C_{A,X}Q_X + C_{A,R}Q_R)}{C_{A,F}Q_F}$
Enzyme productivity (kg_A/g_{Enz})	$PRE = \dfrac{C_{A,F}Q_F \times X/100}{C_{Enz,E}Q_E}$
Adsorbent productivity (kg m^{-3} h^{-1})	$PRA = \dfrac{C_{A,F}Q_F \times X/100}{V_{ads}}$

Table 3. Bi-LDF Steady-State Equivalent TMBR Model Input Parameters

Model Parameters	Operating Conditions	Columns
Pe = 500/column	$T = 55°C$ pH = 4.5	$D_b = 2.6$ cm
$Bi_m = 500$		$L_b = 29$ cm
$k_r = 50.32\ min^{-1}$	$C_F = 80$ g/L	Configuration: 3–2–5–2
$K_{mm} = 23$ g/L	$C_{Enz} = 25–250$ mg/L	$d_p = 320\ \mu m$
$k_{pA} = 1.7\ min^{-1}$ $k_{pB(C)} = 2.5\ min^{-1}$	$t^* = 3.4$ min	
$k_{\mu A} = 0\ min^{-1}$ $k_{\mu B(C)} = 1.5\ min^{-1}$	$Q_{Rec} = Q_4 = 24$ mL/min	
$K_A = 0$ $K_B = 0.43$ $K_C = 0.17$	$\gamma_1 = 0.953$	
$K_{Enz} = 4$ $\varepsilon_p = 0.1$	$\gamma_4 = 0.325$	

$$\gamma_4 < \nu(K_C + \varepsilon_p) = 0.405$$

Safety margins of 1.2 and 1.25 were applied for γ_1 and γ_4, respectively. The γ_1 and γ_4 were set on 0.953 and 0.325, respectively.

The algorithm used in the determination of the reactive–separation regions is presented in Figure 2. The steady-state TMBR model was successively solved for several values of γ_2 and γ_3 within the region between the diagonal $\gamma_2 = \gamma_3$, the horizontal line $\gamma_3 = 0.325$, and the γ_3 axis. The diagonal $\gamma_2 = \gamma_3$ corresponds to a zero feed flow rate, and thus γ_3 must be higher than γ_2. The horizontal branch $\gamma_3 = 0.325$ corresponds to a zero raffinate flow rate.

The starting point (first point in step 1) in the algorithm corresponds to $Q_F = 0.01$ mL/min and $\gamma_2 = 0.325$. The feed flow rate was kept constant and the flow rate in zone 2 was increased gradually starting from the value $\gamma_2 = 0.325$. For any value of flow rate in zone 2 the flow rate in zone 3 was calculated using the mass balance for the feed node, and was translated to the γ_3 form. For each pair of (γ_2, γ_3) the conversion and product purities were estimated. The values that satisfy the conversion and purity criteria were selected to build the reactive–separation region. The values that did not accomplish these requirements were discarded. After the first set of simulations was finished (step 1), the feed flow rate was increased to the next higher value and the same procedure was repeated. The simulation procedure ends with the last (highest) value of the feed flow rate, which gives required product purities and conversion. Above that feed flow rate value the conversion and purity requirements cannot be fulfilled for any pair of values of (γ_2, γ_3).

Influence of the Product Purities on Reactive–Separation Regions. The influence of the required product purities on the SMBR reactive–separation regions was studied. The SMBR unit configuration, model parameters, and operating conditions are presented in Table 3. The enzyme concentration used in this study was 50 mg/L. The product purities requirements were set on 90, 95, and 97% with a reactant minimum conversion of 99%. The obtained reactive–separation regions are presented in Figure 3. The operation of the SMBR at the upper border of each reactive–separation region would lead to raffinate with the required purity (90, 95, and 97%) and extract with purity higher than required. On the other hand, the operation in the lower border leads to extract with the required purity and raffinate with purity higher than required. The conversion was complete (100%) on both borders for each of the reactive–separation regions presented in Figure 3.

The reactive–separation regions expand with decrease of the purity requirements and, in the case of purities of 90 and 95%, the region extends its borders out of the separation region

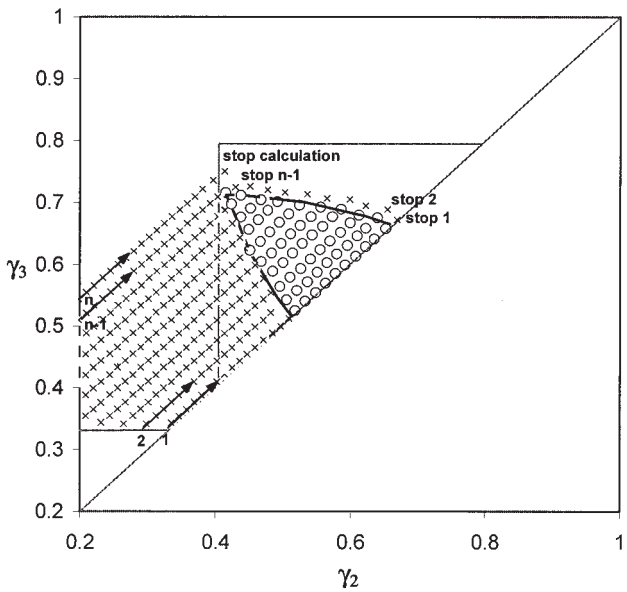

Figure 2. Algorithm for determination of the reactive–separation regions.

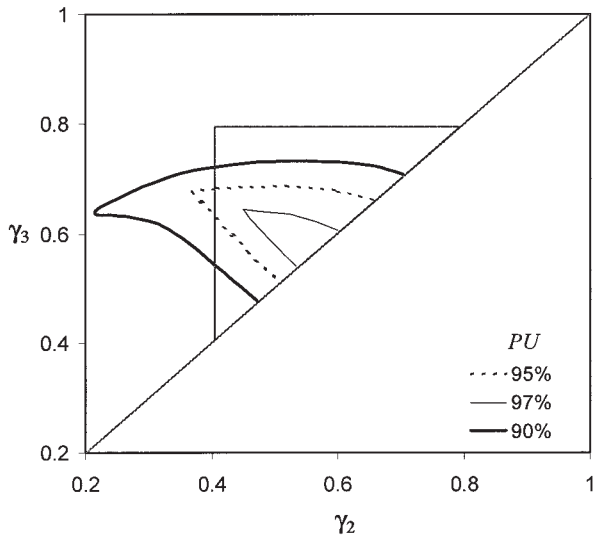

Figure 3. Reactive–separation regions for different product purities in the presence of mass-transfer resistance.

$X_{min} = 99\%$ and $C_{Enz} = 50$ mg/L.

defined for the case of nonreactive separation and no mass-transfer limitation. It is also interesting to observe that the vertex (equal purity in extract and raffinate) moves to lower rather than higher values of γ_3 in the case of 90% product purity restriction.

To better understand this behavior it is important to point out two peculiarities of the SMBR system considered here:

(1) The reaction occurs mainly in zone 3. The sucrose passing to zone 2 is strictly a result of the presence of mass-transfer limitations.

(2) The enzyme is introduced in the system with the eluent. Therefore, there are two zones of different concentrations of enzyme in the system: (a) higher enzyme concentration in zones 1 and 2; and (b) lower enzyme concentrations in zones 3 and 4, resulting from the dilution of the enzyme by the introduction of the feed stream.

In the case of low feed flow rate the concentration of the enzyme is sufficient for complete and almost instantaneous sucrose conversion just at the beginning of zone 3 (only a small part of this zone is used for reaction), and SMBR behaves closely to a nonreactive SMB for separation of fructose/glucose feed mixture.

When the feed flow rate increases, the reactive–separation region extends out of the nonreactive SMB separation region. A higher feed flow rate means a higher quantity of sucrose to be converted and lower enzyme concentration in zone 3. Consequently, the flow rate in zone 3 (γ_3) needs to be lower to achieve both high conversion and adsorption of fructose. Also, the values of γ_2 violate the restrictions defined for a nonreactive SMB, as a result of the allowed product contamination. The glucose would not be completely desorbed in zone 2 and would contaminate the extract. When the allowed contamination increases, from 3 to 10%, the reactive–separation regions expand to the lower values of γ_2.

Influence of the Enzyme Concentration on Reactive–Separation Regions. The influence of the enzyme concentration was studied for 95% product purities restriction and minimum conversion of 99%. For this study the enzyme concentration was varied between 25 and 250 mg/L.

The reactive–separation regions for different enzyme concentrations are presented in Figure 4a. In the same figure, the region obtained in the case of nonreactive SMB for separation of a fructose/glucose mixture, assuming that the unit is fed with completely inverted sucrose (42.08 g/L of glucose and fructose), is also presented.

The vertices move to the region of lower values of γ_2 and γ_3 with decrease of the enzyme concentration in the eluent. The reason for this behavior is connected to the feed flow rate and enzyme concentration and was explained in detail in the previous section.

The reactive–separation region approaches the nonreactive separation region with increasing enzyme concentration. In the case of sufficiently high invertase concentration the reaction is very fast and sucrose conversion is complete at the entrance in zone 3; then the SMBR behavior approaches that of the SMB for separation of glucose/fructose mixture.

The maximum feed can be processed with enzyme concentrations between 50 and 250 mg/L (see Figure 4a). In all these cases the feed flow rate in the vertex is almost the same. Besides the maximum throughput, product purities, and conversion, the enzyme and adsorbent performances are of crucial

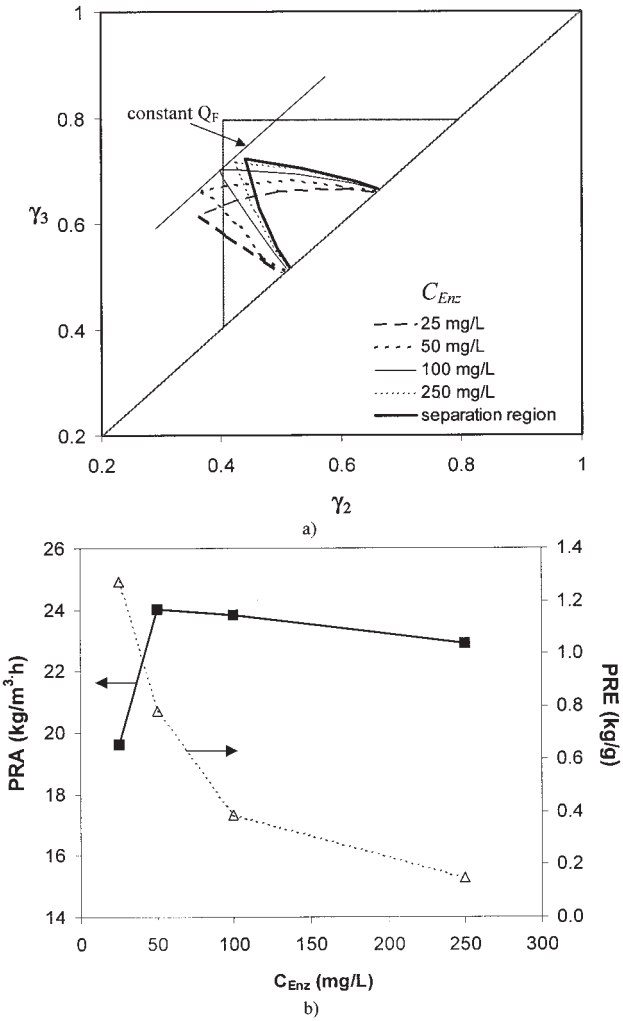

Figure 4. (a) Reactive–separation regions for different enzyme concentrations in the presence of mass-transfer resistance; (b) enzyme productivity (*PRE*) and adsorbent productivity (*PRA*) in the vertexes of the reactive-separation regions for different enzyme concentrations (*PUX* = 95%, *PUR* = 95%, and X_{min} = 99%).

interest. The enzyme and adsorbent productivities (*PRE* and *PRA*, respectively) in the vertices for different enzyme concentrations are presented in Figure 4b. In can be observed that the best performances would be expected for an enzyme concentration around 40 mg/L.

Reactive–separation region in the absence of mass-transfer limitation

To better understand the factors that govern the size and position of reactive–separation regions the SMBR for sucrose inversion was studied in the absence of mass-transfer limitation. The bi-LDF model was used and mass transfer and axial dispersion were eliminated by multiplying the mass-transfer parameters and the Peclet (Pe) number by a factor of 100. The product purity requirements were restricted to 99% because it was previously concluded that one of the reasons for the

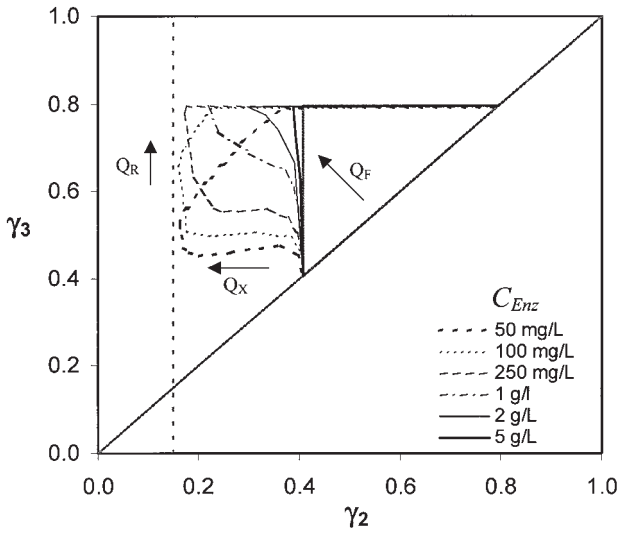

Figure 5. Reactive-separation regions for different enzyme concentrations in absence of mass transfer resistance (*PUX* = 99%, *PUR* = 99%, and X_{min} = 99%).

extension of the borders of SMBR reactive–separation region out of the nonreactive SMB region could be the relaxation of product purities requirements. The product purities of 99% are possible only for very high conversions ($X > 99\%$). The product conversion requirement was kept at the minimum of 99%. Besides, in most cases the conversion in the reactive–separation region border was between 99.7 and 100%. The same net flow rates in zones 1 and 4 as in the case with mass-transfer limitation were used ($\gamma_1 = 0.953$ and $\gamma_4 = 0.325$).

Influence of the Enzyme Concentration on Reactive–Separation Regions. The reactive–separation regions for sucrose inversion in the absence of mass-transfer resistance were determined for enzyme concentrations between 50 mg/L and 5 g/L. The obtained regions are presented in Figure 5. For all enzyme concentrations the reactive–separation regions expand out of the nonreactive separation region (gray triangle), calculated from the equilibrium theory for an SMB for reaction products (glucose and fructose) separation. The minimum γ_2 value and maximum γ_3 value reached by the reactive–separation regions correspond to values calculated with the equilibrium theory, $\gamma_{2\min} = \nu(K_A + \varepsilon_p) = 0.150$ and $\gamma_{3\max} = \nu(K_B + \varepsilon_p) = 0.795$, respectively. All reactive–separation regions share the same upper border, adjacent to the region of impure raffinate. In the case of enzyme concentrations between 50 and 100 mg/L the upper border of the reactive–separation regions is cut along a line that corresponds to almost constant feed flow rate ($\gamma_3 - \gamma_2$) $\approx$ const. With increasing enzyme concentration the regions expand to $\gamma_3 = 0.795$. The lower border of the reactive–separation regions, adjacent to the region of impure extract, moves to higher values of γ_2 and γ_3 with increasing enzyme concentration. For $C_{Enz} > 5$ g/L the enzyme concentration in zone 3, near the feed port, is high enough to instantaneously convert all sucrose introduced in the unit and therefore the SMBR unit would behave as an SMB unit fed with glucose/fructose mixture.

In the following the reasons that lead to the shape and position of the obtained reactive–separation regions will be discussed.

There are two possible reasons for the extension of the reactive–separation region to lower values of γ_2 relative to those calculated for the equivalent nonreactive SMB. The first reason is the rate of the reaction; that is, in the SMBR for sucrose inversion without mass-transfer limitation the SMBR design is governed primarily by the reaction rate. When the reaction is slow both glucose and fructose are produced at some distance from the feed port. This situation can be associated with an SMB in which the point of introduction of the glucose/fructose mixture is moved along zone 3 and part of zone 3 behaves as an extension of zone 2, that is, plays the role of zone 2 (adsorption of fructose). The second reason can be the negligible contamination of 1% of the products allowed. The conversion and product purities were calculated for the operating points laying on a line with constant γ_3 (=0.622), which crosses the reactive–separation region obtained for $C_{Enz} = 250$ mg/L. The conversion and product purities for each point on the line and $C_{Enz} = 250$ mg/L are presented in Figure 6. The raffinate and extract purities of 100% can be obtained just for the values of $\gamma_2 > 0.405$ (that is, $\gamma_{2\min}$ determined according to the equilibrium theory for nonreactive SMB for glucose/fructose separation). The raffinate purity decreases from 100 to 99% when the γ_2 value decreases from $\gamma_2 = 0.405$ to the γ_2 value on the border of the reactive–separation region.

The reactive–separation region for $C_{Enz} = 50$ mg/L and $C_{Enz} = 250$ mg/L together with some operating points inside and outside the regions are presented in Figure 7. The steady-state concentration profiles in the selected points were analyzed to better understand the grounds for the region's shape.

The concentration profiles of the reaction species (*A*, *B*, and *C*) and the enzyme in the operating points 1, 2, and 3 calculated for $C_{Enz} = 50$ mg/L are presented in Figure 8a. For all these points the flow rate in zone 2 is the same (equal γ_2). Moving from point 1 to point 3, the feed flow rate increases, leading to an increase of the concentration of sucrose at the beginning of zone 3 and the residence time decreases because the flow rate in zone 3 increases with increasing feed flow rate. Also, although the enzyme concentration in the eluent is the same, the enzyme concentration in the SMBR decreases going from point 1 to point 3. This decrease in the enzyme concentration is more visible in the reaction zone (zone 3). The rate of the reaction at the entrance of zone 3 decreases in direction to point 3. In the conditions of point 1, because the reaction is fast and the residence time sufficiently long, the complete conversion of sucrose occurs near the feed port. However, the flow rate in zone 3 is not high enough to prevent the passage of glucose in zone 2 and contamination of the extract. This contamination is reduced and products with required purities (99%) are obtained in point 2. At this point the reaction is slower as a result of lower enzyme concentration in zone 3, although all sucrose is still converted until the middle of zone 3. The reaction occurs at a longer distance from the feed port and prevents the passage of glucose in zone 2. In point 3 the reaction becomes so slow that all zone 3 is used for the sucrose inversion. The sucrose is not completely converted until the raffinate port; both products are being produced and contamination of the raffinate by fructose and sucrose can be observed. Only point 2 is inside the reactive–separation region for $C_{Enz} = 50$ mg/L.

The internal concentration profiles for the operating condi-

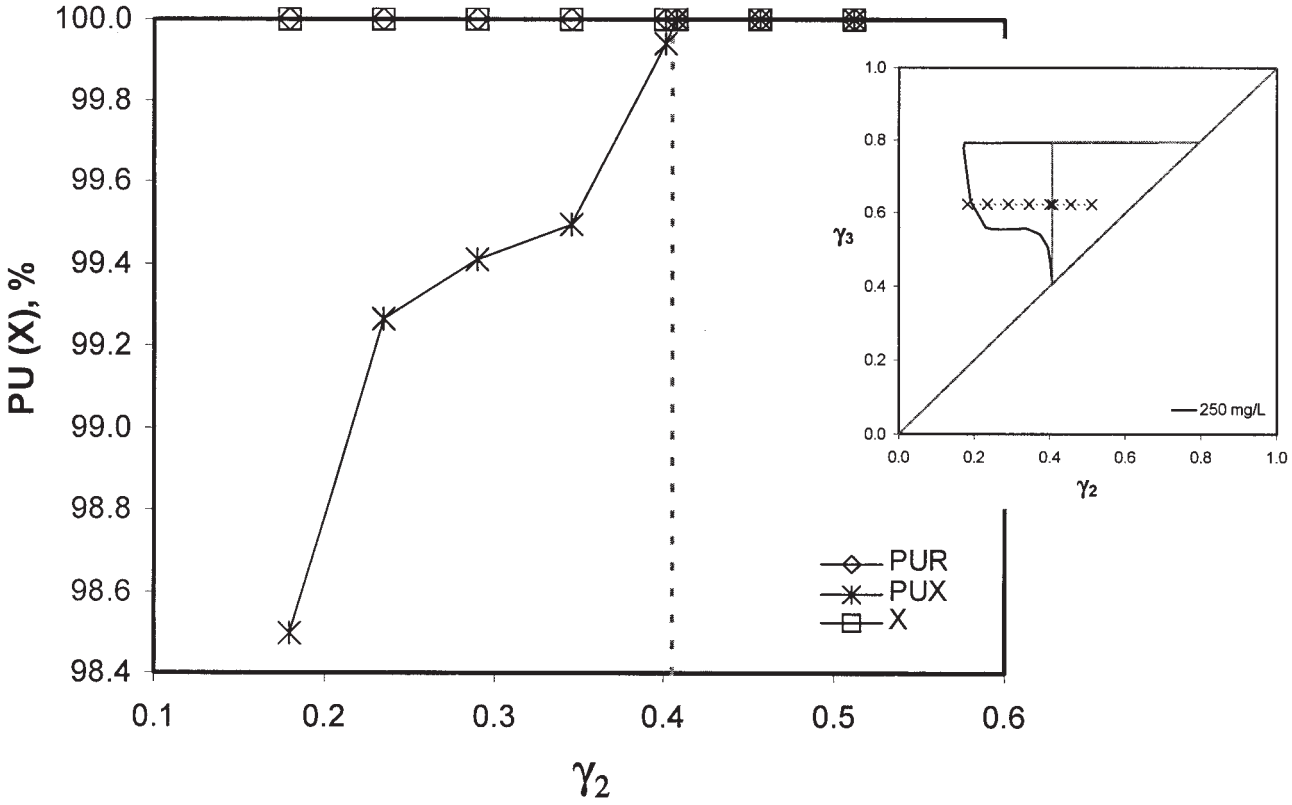

Figure 6. Conversion and product purities in selected operating points along the dashed line corresponding to γ_3 = 0.622, for C_{ENZ} = 250 mg/L.

tions in points 2 and 3 were also calculated for C_{Enz} = 250 mg/L (see Figure 8b). The sucrose concentration at the feed port and the residence time are the same as in the previous case (C_{Enz} = 50 mg/L). In point 2, the reaction is very fast because the enzyme concentration in the SMBR is almost five times higher than that in the previous case and the sucrose concentration at the entrance of reaction zone is unchanged. The sucrose reacts completely very near to the feed port and the flow rate in zone 3 is not high enough to prevent the passage of glucose in zone 2. Also, the reaction is faster when C_{Enz} = 250 mg/L is used together with the operating conditions in point 3. The sucrose does not reach the raffinate port and pure raffinate is obtained. Point 2 is outside and point 3 is inside the reactive–separation region for C_{Enz} = 250 mg/L.

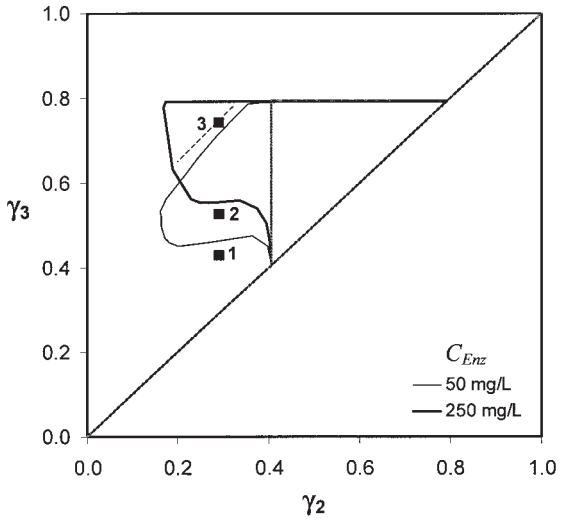

Figure 7. Reactive-separation regions for C_{ENZ} = 50 mg/L and C_{ENZ} = 250 mg/L with some selected points.

Let us see now why the reactive–separation region for C_{Enz} = 50 mg/L is cut along a line that corresponds to almost constant feed flow rate. It was shown before that point 3 does not belong to the reactive–separation region because of the contamination of the raffinate with sucrose and fructose, as a result of incomplete sucrose conversion (that is, insufficiently fast reaction) in zone 3. The same reason is valid for all points along the dashed line presented in Figure 7. The reason for the cutoff of the reactive–separation regions along the line with almost constant feed flow rate is the enzyme concentration in the eluent, which is not sufficiently high to promote complete sucrose conversion before the raffinate port. The points along the dashed line (Figure 7) would belong to the reactive-separation region when the enzyme concentration is increased from 50 to 100 mg/L, as demonstrated in Figure 5.

It would be interesting to analyze the obtained reactive–separation regions in terms of the maximum feed processed, product concentrations and the quantity of the enzyme used. The quantity of feed processed (or sucrose inverted) is directly connected to the difference of the net flow rates in zone 3 and 2 ($\gamma_3 - \gamma_2$). So, we can say that the maximum feed will be processed for enzyme concentration around 250 mg/L (see

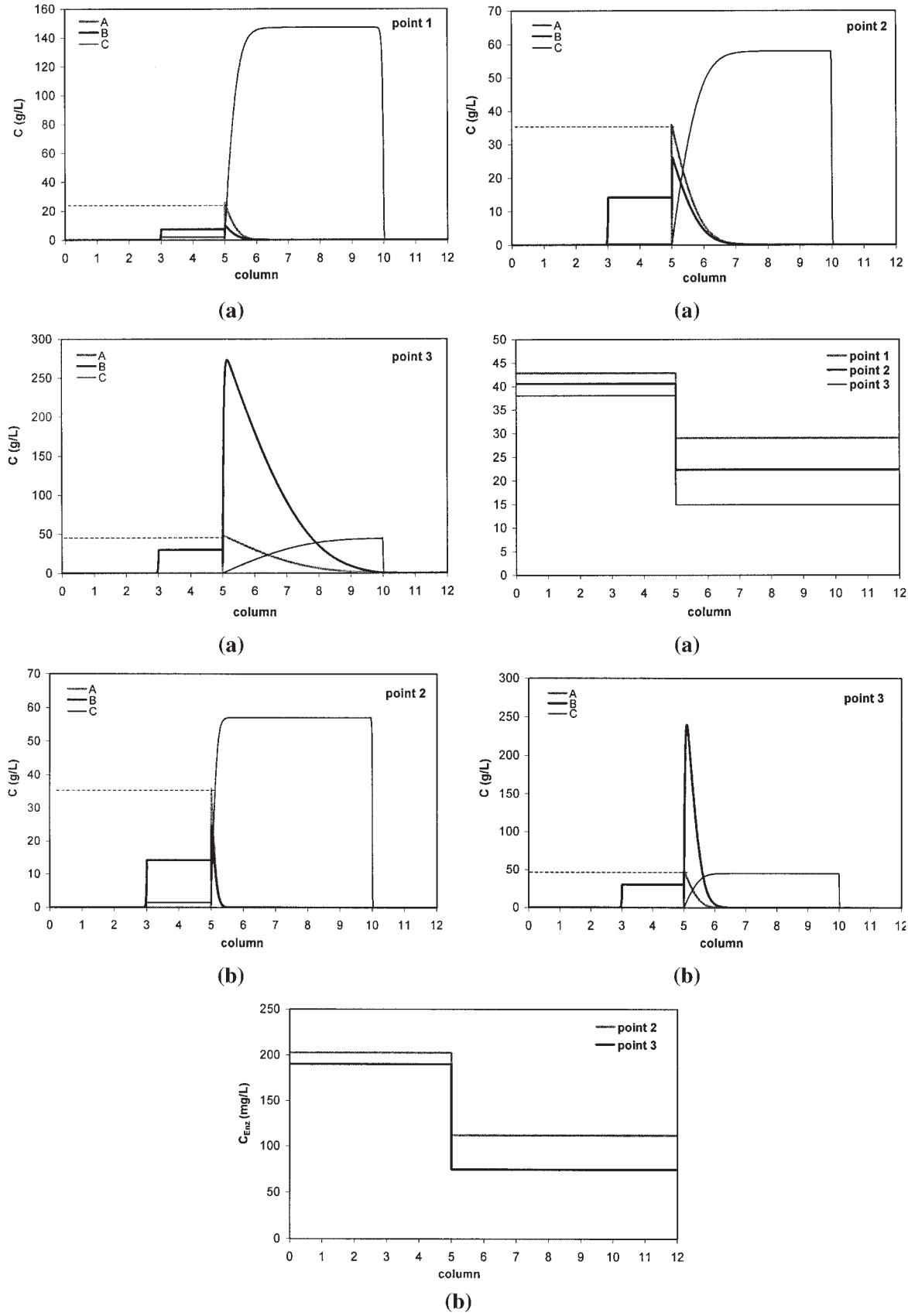

Figure 8. Equivalent TMBR steady-state concentration profiles for points 1–3 from Figure 7.

(a) Points 1–3 and C_{Enz} = 50 mg/L; (b) points 2 and 3 and C_{Enz} = 250 mg/L.

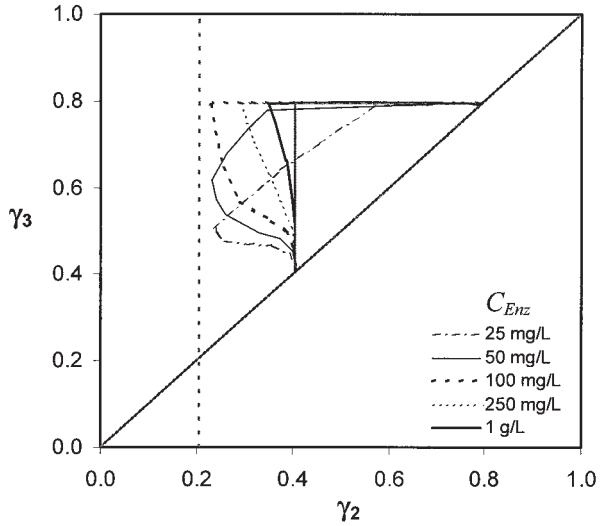

Figure 9. Reactive–separation regions for the case $K_A < K_C < K_B$ (in the absence of mass-transfer resistance) for different enzyme concentrations.

PUX = 99%, *PUR* = 99%, and X_{min} = 99%.

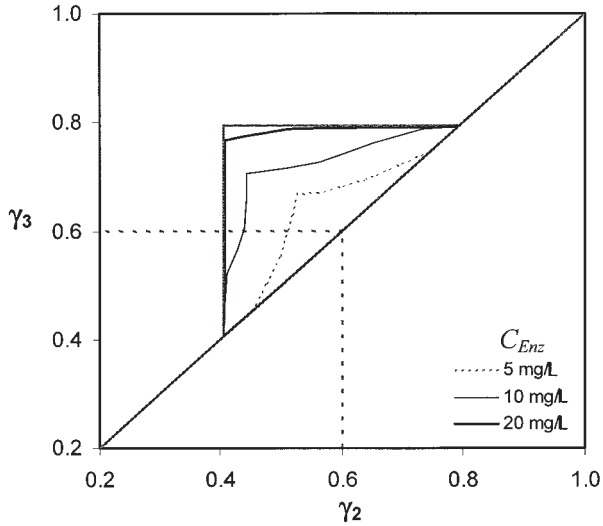

Figure 10. Reactive–separation regions for the case $K_C < K_A < K_B$ (in the absence of mass-transfer resistance) for different enzyme concentrations.

PUX = 99%, *PUR* = 99%, and X_{min} = 99%.

Figure 5). The operating points that correspond to highest feed throughput belong to the region of low values γ_2 (near γ_2 = 0.150) and high values of γ_3 (γ_3 = 0.795). In that region, the products are quite diluted because the flow rates of the extract [which is directly connected to ($\gamma_1 - \gamma_2$)] and raffinate [which is directly connected to ($\gamma_3 - \gamma_4$)] are high. This would imply high cost for recovering the pure glucose and fructose from the extract and raffinate.

Influence of the Reactant Henry Constant on the Reactive–Separation Regions. In the SMBR unit for sucrose inversion, it is assumed that sucrose does not adsorb in the adsorbent particle. The Henry constant of sucrose is equal to zero; therefore, the minimum γ_2 would be for $\varepsilon = 0.4$ and $\varepsilon_p = 0.1$, $\gamma_{2min} = \nu(K_A + \varepsilon_p) = 0.15$. The reactive–separation region for all analyzed enzyme concentration also approaches a value of 0.15.

To better understand the connection between γ_2 (or γ_3) and the Henry constant of the reactant three hypothetical cases for the reactant adsorption parameter were considered: K_A = 0.037, K_A = 0.3, and K_A = 0.57, or in terms of γ values, γ_A = 0.206, γ_A = 0.600, and γ_A = 1.005. In all these cases it was assumed that the reactant enters in the adsorbent particle pores. The Henry constants of the products B and C were those used before: K_B = 0.43 and K_C = 0.17, or in terms of γ values, γ_B = 0.795 and γ_C = 0.405, respectively.

The reactive–separation regions for three cases for the reactant adsorption affinity relative to the products adsorption affinity were determined:

(1) Reactant as less adsorbed component ($K_A < K_C < K_B$)

(2) Reactant as middle adsorbed component ($K_C < K_A < K_B$)

(3) Reactant as most adsorbed component ($K_C < K_B < K_A$)

In Figure 9 the reactive–separation regions for the case $K_A < K_C < K_B$ in the absence of mass-transfer resistance for different enzyme concentrations are presented. This case is very similar to the real one; the only difference is that now sucrose is adsorbed. Once again the reactive–separation region approaches the line γ_2 = 0.206, which corresponds to the one calculated for the reactant A according to the equilibrium theory (γ_A = 0.206).

The reactive–separation regions for the case of reactant as middle adsorbed component ($K_C < K_A < K_B$) are presented in Figure 10. The reaction occurs in both zones 2 and 3 and the SMBR configuration used was 3–3–3–3. The reaction zone (zones 2 and 3) has one column less than in the case $K_A < K_C < K_B$. This configuration was selected because the value of K_C (0.205) is exactly the middle value between K_A (0.795) and K_B (0.405), and therefore, neither of zones 2 or 3 is privileged in

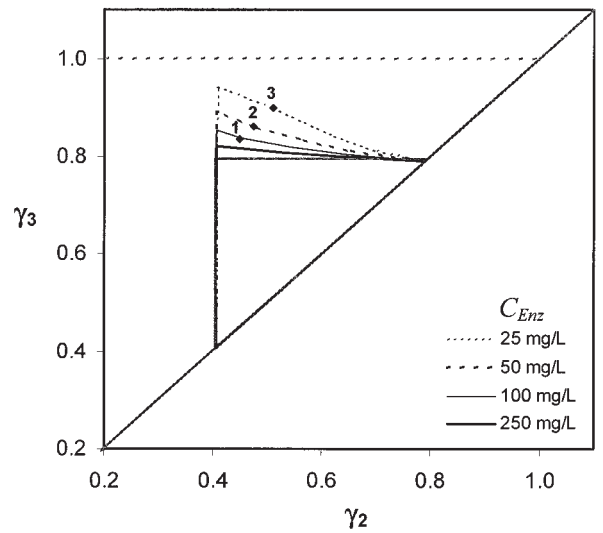

Figure 11. Reactive–separation regions for the case $K_C < K_B < K_A$ (in the absence of mass-transfer resistance) for different enzyme concentrations.

PUX = 99%, *PUR* = 99%, and X_{min} = 99%.

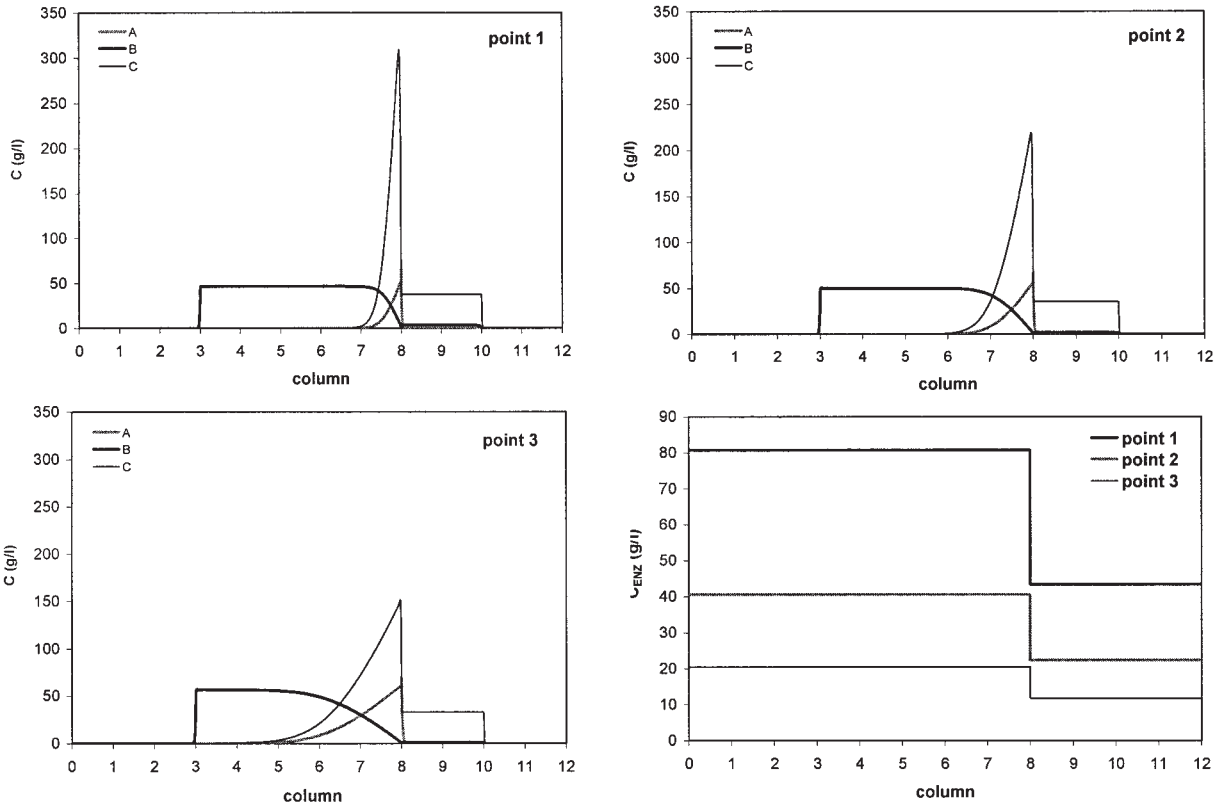

Figure 12. Equivalent TMBR steady-state concentration profiles for points 1–3.

terms of the reaction. The enzyme concentration was varied between 5 and 20 mg/L. For enzyme concentration above 20 mg/L the reactive–separation region matches with the separation region of products B and C. It can be seen that enzyme concentrations lower than those in the previous case are used.

For $K_C < K_B < K_A$ the reactive–separation regions for different enzyme concentrations are presented in Figure 11. The 3–5–2–2 configuration was used because the reaction takes place just in zone 2. The enzyme concentration used in the calculation was between 25 and 250 mg/L. For all enzyme concentrations the border of the reactive–separation regions (with 99% extract end raffinate purities) with the region of pure raffinate only is $\gamma_2 = 0.405$. On the other hand, the border with the region of pure extract extends only to values of $\gamma_3 > 0.795$. When higher enzyme concentrations are used the reaction is fast and occurs at the end of zone 2, near the feed port; thus the system behaves closely to the nonreactive SMB for B/C separation.

The internal steady-state concentration profiles for points 1, 2, and 3 (see Figure 11) are presented in Figure 12. These points correspond to equal feed flow rates, but different enzyme concentrations: point 1, $C_{Enz} = 100$ mg/L; point 2, $C_{Enz} = 50$ mg/L; and point 3, $C_{Enz} = 25$ mg/L. It can be seen that when the enzyme concentration decreases the reaction becomes slower, both B and C are produced more distant from the feed port, and thus a higher flow rate in zone 2 has to be used to prevent the contamination of the extract (>1%) with the product C. The flow rate in zone 3 would also be higher because the feed flow rate is constant for all three points. The opposite will occur when the reaction is fast (point 1); lower values of flow rate in zones 2 and 3 have to be used to ensure the adsorption of component B and prevent the contamination of the raffinate.

Once again the extension of the reactive–separation region out of the nonreactive separation for the cases $K_A < K_C < K_B$ and $K_C < K_B < K_A$ is related with the reaction rate and small contamination of the products allowed. In both cases significantly higher feed throughput can be used. Also this throughput can be processed with the lower values of the enzyme concentration used, 100 mg/L in the case $K_A < K_C < K_B$ and 25 mg/L in the case $K_C < K_B < K_A$. Additional analysis would be needed in terms of product concentration, that is, the costs for the recovery of products (B and C) from the extract and raffinate, respectively.

The SMBR for sucrose inversion is quite complex because the enzyme is not immobilized and its concentration in zones 1 and 2 is different from that in zones 3 and 4 because of the dilution with the feed stream. Therefore, even when a constant enzyme concentration in the eluent is used, any point in the reactive–separation region is characterized by different enzyme concentrations, that is, different reaction rates. Also, the reaction kinetic is described with the Michaelis–Menten equation, according to which the rate of the reaction changes both with enzyme and sucrose concentration in the reaction zone. All this introduces some complexity to the analysis and prediction of the reactive–separation region.

In the next section some simplifications will be introduced for an SMBR with A $\rightarrow$ B + C type of reaction.

Table 4. LDF Steady-State Equivalent TMBR Model Equations

Mass balance in the inter-particle liquid phase in zone j

$$\frac{\gamma_j}{\mathrm{Pe}_j}\frac{d^2C_{i,j}}{dx^2} - \gamma_j\frac{dC_{i,j}}{dx} - \nu\alpha_{h_{i,j}}(K_i'C_{i,j} - \langle q\rangle_{i,j}) + \sigma_i\mathrm{Da}_jC_{A,j} = 0 \quad (i = A, B, C)$$

where

$$\sigma_i = \begin{cases} -1 & \text{if } i \text{ is } A \\ +0.526 & \text{if } i \text{ is } B \text{ or } C \end{cases}$$

Mass balance in the adsorbent particles in zone j

$$\frac{\partial\langle q\rangle_{i,j}}{\partial x} + \alpha_{h_{i,j}}[K_i'\langle C\rangle_{i,j} - \langle q\rangle_{i,j}] = 0$$

$$K' = K + \varepsilon_p$$

Boundary conditions for a given zone j are

$$C_{i,j}^{in} = C_{i,j}(0) - \frac{1}{\mathrm{Pe}_j}\frac{\partial C_{i,j}}{\partial x} \qquad \frac{\partial C_{i,j}}{\partial x}(1) = 0 \qquad (i = A, B, C)$$

$$\langle q\rangle_{i,j}(1) = \langle q\rangle_{i,j+1}(0) \qquad (i = A, B, C)$$

Dimensionless groups

$$\gamma_j = \frac{U_{F_j}'}{U_S} \qquad \mathrm{Pe}_j = \frac{U_{F_j}'L_j}{D_{axj}} \qquad \nu = \frac{(1-\varepsilon)}{\varepsilon}$$

$$\alpha_{h_{i,j}} = \frac{k_{h_i}L_j}{U_S} \qquad \sigma_i = \frac{\text{Mol. weight of } B \text{ (or } C)}{\text{Mol. weight of } A} \qquad \mathrm{Da}_j = \frac{L_jk_r}{U_S}$$

Node mass balances

Eluent node
$$C_{i,1}^{in} = \frac{Q_4'}{Q_1'}C_{i,4}(1) + \frac{Q_E}{Q_1'}C_{i,E}$$

Feed node
$$C_{i,3}^{in} = \frac{Q_2'}{Q_3'}C_{i,2}(1) + \frac{Q_F}{Q_3'}C_{i,F}$$

Extract node
$$C_{i,2}^{in} = C_{i,1}(1)$$

Raffinate node
$$C_{i,4}^{in} = C_{i,3}(1)$$

SMBR for A → B + C: General Case

The SMBR where reactant A is irreversibly converted to products B and C (A → B + C) is considered. The reaction kinetics is of first-order linear reaction kinetics, catalyzed with enzyme immobilized on the adsorbent particles. All species are adsorbed and exhibit linear adsorption equilibrium isotherms.

For the purpose of modeling the SMBR was assumed as an equivalent TMBR (Figure 1b) operating in steady state. The mathematical model considers plug flow for the liquid and solid phases, the presence of internal mass transfer described by the linear driving force (LDF) model, and linear adsorption isotherm. This model is simpler than the bi-LDF steady-state TMBR model used previously. The LDF steady-state TMBR model equations are summarized in Table 4. Minceva et al.[35] recently proposed an analytical solution for this model.

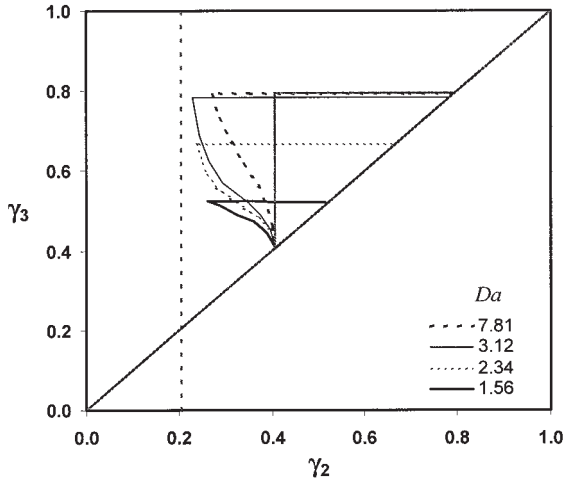

Figure 13. Reactive–separation regions for first-order reaction A → B + C, in the case $K_A < K_C < K_B$ (in the absence of mass-transfer resistance) for different Da numbers.

PUX = 99%, *PUR* = 99%, and $X_{\min}$ = 99%.

The SMBR configuration, column geometry, and operating conditions, together with the adsorption equilibrium, mass transfer, and reaction parameters for the reactant A and products B and C are presented in Table 5.

The reactive–separation regions were determined in the absence of mass-transfer limitation; the internal mass transfer and axial dispersion were eliminated by multiplying the mass-transfer parameter and Pe number by a factor of 100. The product purities were set to 99% and the conversion at a minimum of 99%.

Three different cases for the reactant adsorption affinity relative to those of products B and C were considered:

(1) Reactant as less adsorbed component ($K_A < K_C < K_B$)

(2) Reactant as middle adsorbed component ($K_C < K_A < K_B$)

(3) Reactant as most adsorbed component ($K_C < K_B < K_A$)

The Henry constants of the products B and C were $K_B = 0.43$ ($\gamma_B = 0.795$) and $K_C = 0.17$ ($\gamma_C = 0.405$). The reactant A adsorption parameters were: $K_A = 0.037$, $K_A = 0.3$, and $K_A = 0.57$, or $\gamma_A = 0.206$, $\gamma_A = 0.600$, and $\gamma_A = 1.005$, respectively. For all three cases of reactant adsorption affinity the SMBR configuration 3–3–3–3 was selected and the γ_1 and γ_4 were set on 0.953 and 0.325, respectively.

The reactive–separation regions for the case of reactant as less adsorbed component, $K_A < K_C < K_B$ (0.037 < 0.17 < 0.43), for different Damköhler (Da) numbers are presented in Figure 13. The reactant A is carried out with the liquid phase in the direction of the raffinate port and the reaction occurs strictly in zone 3 and the Da number in this zone is thus the

Table 5. LDF Steady-State Equivalent TMBR Model Input Parameters

Model Parameters	Operating Conditions	Columns
Pe = 500/column	t^* = 3.4 min	D_b = 2.6 cm
k_r = 0.61 min^{-1}	C_F = 80 g/L	L_b = 29 cm
k_{hB} = 1.32 min^{-1} k_{hC} = 1.89 min^{-1}	$Q_{Rec} = Q_4$ = 24 mL/min	Configuration: 3–3–3–3
K_B = 0.43 K_C = 0.17	γ_1 = 0.953	
ε_p = 0.1	γ_4 = 0.325	

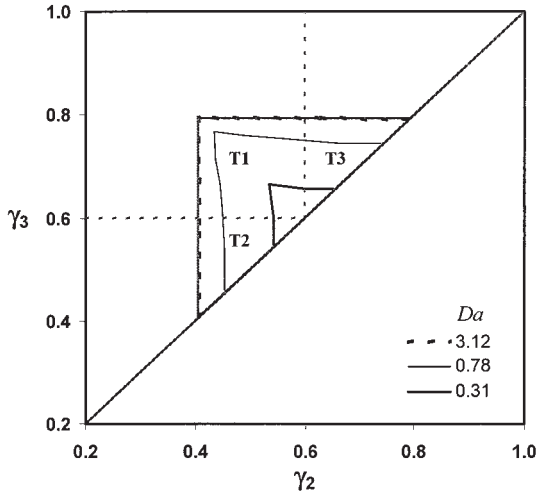

Figure 14. Reactive–separation regions for first-order reaction A → B + C, in the case $K_C < K_A < K_B$ (in the absence of mass-transfer resistance) for different Da numbers.

PUX = 99%, *PUR* = 99%, and X_{min} = 99%.

controlling parameter. The reactive–separation regions were determined for Da numbers 1.56, 2.34, 3.12, and 7.81 (see Figure 13). For all values of the Da number the reactive–separation regions approaches the line $\gamma_2 = 0.206$, which corresponds to $\gamma_A = 0.206$, calculated according to the equilibrium theory. The border of the region of pure extract only is defined by a constant value of γ_3, which increases with the increase of Da number and approaches $\gamma_3 = \gamma_B = 0.795$ when the reaction is fast enough. For low values of Da the reaction is slow, and a lower flow rate in zone 3 must be used to increase the residence time of the reactant A and ensure conversion higher than 99% and prevent the contamination of the raffinate with the product B. With increasing Da number the reaction becomes faster and a higher flow rate in zone 3 can be used. Once again, in the case of sufficiently high Da numbers, the reactant is completely converted near the feed port and the reactive separation region matches the equivalent nonreactive SMB separation region.

In Figure 14 the reactive–separation regions for the case $K_C < K_A < K_B$ (0.17 < 0.3 < 0.43) for different Da numbers 0.31, 0.78, and 3.12 are presented. The reaction takes place in zone 2 (region T2), zone 3 (region T3), and both zones 2 and 3 (region T1). For Da = 3.12 the reactive–separation region matches the separation region of products B and C. The case of middle adsorbed reactant is analyzed in detail by Fricke and Schmidt-Traub[33] and Lode et al.[34] They developed explicit design criteria for the reactant conversion as a function of the flow rate ratios as well as of the Da numbers within zones 2 and 3 for a constant degree of reactant conversion.

The influence of the Da number (that is, reaction rate constant) on the reactive–separation regions shape and position for the case $K_C < K_B < K_A$ (0.17 < 0.43 < 0.57) is presented in Figure 15. The reactant, as most adsorbed component, is carried with the solid phase in the direction of the extract port and thus does not enter zone 3. In the absence of mass-transfer resistance the reaction takes place just in zone 2; the Da number in this zone is thus the controlling parameter. The reactive–separation regions were determined for Da numbers 1.56, 2.34, 3.12, and 7.81 (see Figure 15). The border of the reactive–separation regions with the region of pure raffinate only is defined by a constant value of γ_2, which decreases with the increment of Da number and approaches $\gamma_2 = \gamma_C = 0.405$ when the reaction becomes fast enough. When the reaction is slow (low values of Da) a higher flow rate in zone 2 must be used to prevent the contamination of the extract with the product C. On other hand with increasing Da number the reaction becomes faster and a lower flow rate in zone 2 can be used.

The border of the reactive–separation regions with the region of pure extract only goes beyond the γ_3 value calculated from the equilibrium theory for nonreactive SMB, that is, $\gamma_3 = \gamma_B = 0.795$. Because the product purities are set at 99%, a higher flow rate in zone 3 can be used.

Conclusions

The design of a simulated moving-bed rector (SMBR) for an irreversible reaction, A → B + C, was studied. The steady-state equivalent true moving-bed reactor (TMBR) analogy was implemented in the algorithm used for determination of the reactive–separation regions. Two reactive systems were considered: (1) sucrose inversion, with enzyme introduced in the unit through the eluent stream and Michaelis–Menten reaction kinetics, and (2) A → B + C reaction, with immobilized enzyme and linear reaction kinetic law.

The bi-LDF equivalent TMBR model was used to study the product purities and the effect of enzyme concentration on the reactive–separation regions of SMBR for sucrose inversion in the presence of mass-transfer resistance. Because of the relaxation of the product purity requirements the reactive–separation region expands out of the nonreactive SMB separation region, in the direction of lower values of net-flow rate in zones 2 and 3. The same feed throughput could be processed for different enzyme concentrations and constant product purities constraint (95%). This information is very important for the minimization

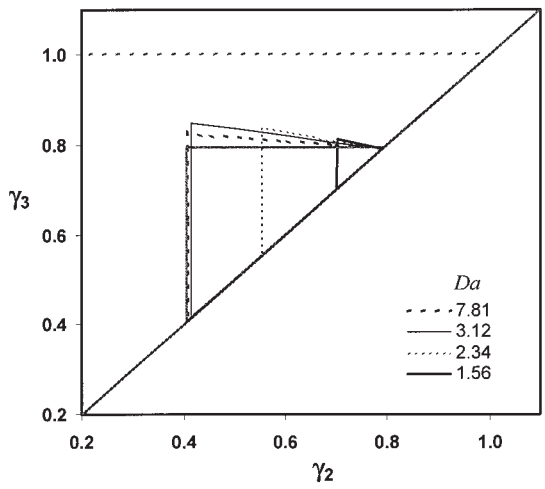

Figure 15. Reactive–separation regions for first-order reaction A → B + C, in the case $K_C < K_B < K_A$ (in the absence of mass-transfer resistance) for different Da numbers.

PUX = 99%, *PUR* = 99%, and X_{min} = 99%.

of the enzyme inventory. The reactive–separation regions were also determined in equilibrium conditions (absence of mass-transfer resistance). Under this condition the regions spread to values of γ_2 near $\gamma_{2\min} = \nu(K_A + \varepsilon_p) = 0.150$ with the increase of the enzyme concentration in the eluent. The main reasons for this behavior are the rate of sucrose conversion in the reaction zone (zone 3) and the small allowed impurity (1%) in the extract and raffinate streams. The reactant adsorption affinity relative to that of the products influences the shape and the position of the reactive–separation region.

In the case of SMBR for general reaction A $\rightarrow$ B + C, with immobilized enzyme and linear reaction kinetic law, special attention was given to the influence of the reactant (A) adsorption affinity on the reactive–separation regions. In the absence of mass-transfer resistance and for given conversion and product purity, the size of the reactive–separation regions is governed by the rate of the reaction. In the cases of reactant (A) as the less adsorbed and the most adsorbed species the regions expand out of the separation regions in the direction of lower γ_2 and higher γ_3 values, respectively. Once again the expansion of the reactive–separation regions out of the equivalent nonreactive SMB for products B/C separation results from the rate of the reaction and small impurity allowed in the product streams.

Acknowledgments

This work was financially supported by FCT (Fundação para a Ciência e Tecnologia, Portugal), Project POCTI/EQU 44515/2002.

Notation

Bi_m = mass Biot number
C = bulk fluid phase concentration, kg/m^3
$\langle C_p \rangle$ = pore fluid phase concentration averaged over the particle volume, kg/m^3
Da = Damköhler number
D_{ax} = axial dispersion coefficient, m^2/s
D_b = column diameter, m
d_p = diameter of adsorbent particle, m
k = mass-transfer constant, s^{-1}
K = adsorption constant as defined in the bi-LDF approximation
K' = adsorption constant as defined in the LDF approximation
k_f = film mass-transfer coefficient, m/s
k_r = rate constant of the inversion reaction kinetics, kg$_A$/kg$_{Enz}$ s^{-1}
K_{Enz} = adsorption constant of enzyme invertase onto adsorbent resin
K_{mm} = Michaelis–Menten constant, kg/m^3
L_b = column length, m
Lj = zone length, m
Pe = Peclet number
PRA = adsorbent productivity, kg m^{-3} h^{-1}
PRE = enzyme productivity, kg$_A$/g$_{Enz}$
PUR = raffinate purity, %
PUX = extract purity, %
$\langle q \rangle$ = adsorbed phase concentration averaged over a homogeneous solid, kg/m^3
$\langle\langle q \rangle\rangle$ = adsorbed phase concentration averaged over a bidisperse particle, kg/m^3
Q = volumetric flow rate in a SMBR, m^3/s
Q' = volumetric flow rate in a TMBR, m^3/s
R_j = reaction rate law, kg m^{-3} s^{-1}
R_p = particle radius, m
t = time, s
t^* = switching time or rotation period, s
T = temperature, K
U_F = interstitial fluid velocity in a SMBR, m/s
U'_F = interstitial fluid velocity in a TMBR, m/s
U_S = interstitial solid velocity in a TMBR, m/s
x = dimensionless space co-ordinate in TMBR-based model
X = reaction conversion, %

Greek letters

α = number of mass-transfer or reaction rate units
γ = ratio between fluid and solid interstitial velocities in a TMBR
ε = bed porosity
ε_p = adsorbent particle porosity
ν = ratio between solid and fluid volumes in a column
σ = stoichiometric reaction parameter

Indices

1, . . . , 4 = index to indicate TMB/SMB zones
A = sucrose
B = fructose
C = glucose
Enz = enzyme
E = eluent
F = feed
h = referring to a homogeneous solid
i = chemical species
in = at the inlet of a column (superscript)
j = TMB zone
p = referring to the pores of a bidisperse adsorbent
r = reaction
R = raffinate
X = extract
μ = referring to the microparticles of a bidisperse adsorbent

Literature Cited

1. Kulprathipanja S. *Reactive Separation Processes.* New York, NY: Taylor & Francis; 2002.
2. Zabransky RF, Anderson RF. *Simulated Moving Bed Alkylation Process*. U.S. Patent No. 4 049 739; 1977.
3. Kawase M, Suzuki TB, Inoue K, Yoshimoto K, Hashimoto K. Increased esterification conversion by application of the simulated moving-bed reactor. *Chem Eng Sci.* 1996;51:2971-2976.
4. Mazzotti M, Kruglov A, Neri B, Gelosa D, Morbidelli M. Continuous chromatographic reactor: SMBR. *Chem Eng Sci.* 1996;51:1827-1836.
5. Strohlein G, Lode F, Mazzotti M, Morbidelli M. Design of stationary phase properties for optimal performance of reactive simulated-moving-bed chromatography. *Chem Eng Sci.* 2004;59:4951-4956.
6. Yu W, Hidajat K, Ray AK. Modeling, simulation, and experimental study of a simulated moving bed reactor for the synthesis of methyl acetate ester. *Ind Eng Chem Res.* 2003;42:6743-6754.
7. Lode F, Houmard M, Migliorini C, Mazzotti M, Morbidelli M. Continuous reactive chromatography. *Chem Eng Sci.* 2001;56:269-291.
8. Zhang Z, Hidajat K, Ray AK. Application of simulated countercurrent moving-bed chromatographic reactor for MTBE synthesis. *Ind Eng Chem Res.* 2001;40:5305-5316.
9. Kawase M, Inoue Y, Araki T, Hashimoto K. Simulated moving-bed reactor for production of bisphenol A. *Catal Today.* 1999;48:199-209.
10. Silva VMTM. *Diethylacetal Synthesis in Simulated Moving Bed Reactor*. PhD Thesis. Porto, Portugal: University of Porto; 2003.
11. Bjorklund MC, Carr RW. Simulated countercurrent moving bed chromatographic reactor: A catalytic and separative reactor. *Catal Today.* 1995;25:159.
12. Ray AK, Carr RW, Aris R. Simulated countercurrent moving bed chromatographic reactor: A novel reactor–separator. *Chem Eng Sci.* 1994;49:469-480.
13. Bjorklund MC, Carr RW. Enhanced methanol yields from the direct partial oxidation of methane in a simulated countercurrent moving bed chromatographic reactor. *Ind Eng Chem Res.* 2002;41:6528-6536.
14. Tonkovich ALY, Carr RW. Simulated countercurrent moving-bed chromatographic reactor for the oxidative coupling of methane: Experimental results. *Chem Eng Sci.* 1994;49:4647-4656.
15. Bjorklund MC, Kruglov AV, Carr RW. Further studies of the oxidative coupling of methane to ethane and ethylene in a simulated countercurrent moving bed chromatographic reactor. *Ind Eng Chem Res.* 2001;40:2236-2242.
16. Hashimoto K, Adachi S, Noujima H, Ueda Y. A new process combining adsorption and enzyme reaction for producing higher-fructose syrup. *Biotechnol Bioeng.* 1983;25:2371-2393.
17. Borges da Silva E, de Souza AAU, de Souza SGU, Rodrigues AE.

Simulated moving bed technology in the reactive process of glucose isomerization. *Adsorption.* 2005;11:847-851.
18. Zhang Y, Hidajat K, Ray AK. Optimal design and operation of SMB bioreactor: Production of high fructose syrup by isomerization of glucose. *Biochem Eng J.* 2004;21:111-121.
19. Toumi A, Engell S. Optimization-based control of a reactive simulated moving bed process for glucose isomerization. *Chem Eng Sci.* 2004; 59:3777-3792.
20. Meurer M, Altenhöner U, Strube J, Untiedt A, Schmidt-Traub H. Dynamic simulation of a simulated-moving-bed chromatographic reactor for the inversion of sucrose. *Starch.* 1996;48:452-457.
21. Barker PE, Ganetsos G, Ajongwen J, Akintoye A. Bioreaction separation on continuous chromatographic systems. *Chem Eng J/Biochem Eng J.* 1992;50:B23-B28.
22. Azevedo DCS, Rodrigues AE. Design methodology and operation of a simulated moving bed reactor for the inversion of sucrose and glucose–fructose separation. *Chem Eng J.* 2001;82:95-107.
23. Hashimoto K, Adachi S, Shirai Y. Development of new bioreactors of a simulated moving-bed type. In: Ganetsos G, Barker PE, eds. *Preparative and Production Scale Chromatography.* New York, NY: Marcel Dekker; 1993:395-419.
24. Shieh MT, Barker PE. Saccharification of modified starch to maltose in a semicontinuous countercurrent chromatographic reactor–separator (SCCR-S). *J Chem Technol Biotechnol.* 1995;63:125-134.
25. Shieh MT, Barker PE. Combined bioreaction and separation in a simulated counter-current chromatographic bioreactor–separator for the hydrolysis of lactose. *J Chem Technol Biotechnol.* 1996;66:265-278.
26. Kawase M, Pilgrim A, Araki T, Hashimoto K. Lactosucrose production using a simulated moving bed reactor. *Chem Eng Sci.* 2001;56: 453-458.
27. Migliorini C, Fillinger M, Mazzotti M, Morbidelli M. Analysis of simulated moving-bed reactors. *Chem Eng Sci.* 1999;54:2475-2480.
28. Dünnebier G, Fricke J, Klatt K-U. Optimal design and operation of simulated moving bed chromatographic reactors. *Ind Eng Chem Res.* 2000;39:2290-2304.
29. Subramani HJ, Hidajat K, Ray AK. Optimization of reactive SMB and Varicol systems. *Comput Chem Eng.* 2003;27:1883-1901.
30. Zhang ZY, Hidajat K, Ray AK. Multiobjective optimization of simulated countercurrent moving bed chromatographic reactor (SCMCR) for MTBE synthesis. *Ind Eng Chem Res.* 2002;41:3213-3232.
31. Yu W, Hidajat K, Ray AK. Optimal operation of reactive simulated moving bed and Varicol systems. *J Chem Technol Biotechnol.* 2003; 78:287-293.
32. Biressi G, Ludemann-Hombourger O, Mazzotti M, Nicoud R-M, Morbidelli M. Design and optimisation of a SMB unit: Role of deviations from equilibrium theory. *J Chromatogr A.* 2000;876:3-15.
33. Fricke J, Schmidt-Traub H. A new method supporting the design of simulated moving bed chromatographic reactors. *Chem Eng Process.* 2003;42:237-248.
34. Lode F, Mazzotti M, Morbidelli M. Comparing true countercurrent and simulated moving-bed chromatographic reactors. *AIChE J.* 2003; 49:977-990.
35. Minceva M, Silva VMT, Rodrigues AE. New analytical solution for reactive SMB in presence of mass transfer resistance. *Ind Eng Chem Res.* 2005;44;5246-5255.
36. Meurer M, Altenhöner U, Strube J, Schmidt-Traub H. Dynamic simulation of simulated-moving-bed chromatographic reactors. *J Chromatogr A.* 1997;769:71-79.
37. Santos MML. *Produção de Dextrano e Frutose a partir da Sacarose com Leuconostoc mesenteroides NRRL B512(f).* PhD Thesis. Porto, Portugal: University of Porto; 1999.
38. gPROMS v2.3.1 User Guide. London, UK: Process System Enterprise Ltd.; 2004.
39. Ruthven DM. *Principles of Adsorption and Adsorption Processes.* New York, NY: Wiley; 1984.

Manuscript received Nov. 12, 2004, and revision received Feb. 15, 2005.